Journal of the Serbian Chemical Society
JSCS-info@shd.org.rs • www.shd.org.rs/JSCS
J. Serb. Chem. Soc. *87* (12) 1381–1393 (2022)
JSCS–5601
Original scientific paper
Published 14 December 2022

3D-QSAR and molecular docking studies of aminothiazole derivatives as Lim kinase 1 inhibitors

JING-XUAN HOU, QING-SHAN GU, MEI-QI SHI, HUI GAO, LU ZHENG* and QING-KUN WU**

School of Pharmacy, Jiangsu Ocean University, Jiangsu, 320000, P.R. China

(Received 10 May, revised 14 July, accepted 23 September 2022)

Abstract: Lim kinase (Limk), as an important cytoskeletal regulator, plays an important role in cancer manifestations and neuronal diseases. Limk1 is a member of the Limk family, which is mainly involved in the invasion and metastasis of tumor cells and is abnormally expressed in a variety of cell carcinoma tissues. In this paper, a series of Limk1 inhibitors with aminothiazole skeleton were used to design potent and efficient Limk1 inhibitors by computational approaches. Firstly, the 3D-QSAR model was constructed, and both CoMFA and CoMSIA models have good correlation and prediction ability. The binding requirements between ligand and receptor protein were then further explored through molecular docking, including the critical forces between Limk1 inhibitors and active site residues. Finally, based on the 3D-QSAR model and molecular docking results analysis, three new compounds with theoretically better activity were designed and their ADME properties were predicted.

Keywords: cancer; CoMFA; CoMSIA; computational drug design.

INTRODUCTION

Invasiveness and metastasis are essential features of malignant tumours and two of the most important causes of death in cancer patients.[1] Limk is known to regulate the conversion of filamentous actin (F-actin) into globular actin (G--actin) by phosphorylation of cofilin substrates and control microtubule dynamics during cell cycle interphase.[2] Due to its associated activity, Limk is involved in many cellular physiological functions, and its dysregulation may lead to cancers and viral infections.[1,3,4] Numerous studies have confirmed that Limk is highly expressed in a variety of human tumours, particularly in highly aggressive tumours.

Members of the Limk family include Limk1 and Limk2, which are characterized by their dual serine/threonine and tyrosine kinase activities. They show

* Corresponding authors. E-mail: (*)zhel-123@163.com; (**)qingkunwuchem@163.com
https://doi.org/10.2298/JSC220510076H

significant similarity in primary amino acid sequences (55 %) and more similarity (72 %) at the level of their kinase structural domains and ATP binding sites.[5] However, the subcellular localization of the two is different, suggesting that they have different roles in tumor cells. Limk1 is mainly involved in the invasion and metastasis of tumor cells,[6] and its phosphorylation can induce cytoskeletal actin dynamics and microtubule depolymerization,[7] so it has abnormal expression in many kinds of tumors.[8,9] Therefore, Limk1 is considered as a therapeutic target to interfere with tumor proliferation, invasion and metastasis.

In 2008, Bristol Myers Squibb disclosed a (BMS-3, Fig. 1) and b (BMS-5) as the first class of Limk1 inhibitors, however their mechanism of action is not yet known.[10] In 2011, Sleebs *et al.* identified c from a series of 5,6-substituted 4-aminothieno[2,3-*d*]pyrimidines, and it had potential for drug-like properties optimization.[11] In 2015, Yin *et al.* identified bisarylurea compounds d and e (SR--11124 and SR-11157), however their application in indications has not been reported.[12] In the same year, starting from a series of aminothiazole skeletons, Charles *et al.* reported Limk1 inhibitors f and g (CRT0105446 and CRT0105950) and follow-up investigation found that rhabdomyosarcoma, neuroblastoma and kidney cancer cells were all significantly sensitive to both of them.[13,14] In 2020, Zhang *et al*. discovered the second generation tyrosine kinase inhibitor h (Dasatinib), which also had a strong inhibitory effect on Limk1.[15] Although a large number of compounds that bind to the ATP pocket of Limk1 have been designed and tested in recent years for their ability to affect Limk1 mediated cofilin phosphorylation and microtubule stability, the clinical achievement of such drugs is limited. Therefore, more Limk1 inhibitors with less side effects and higher efficiency need to be developed to meet the unmet clinical needs.

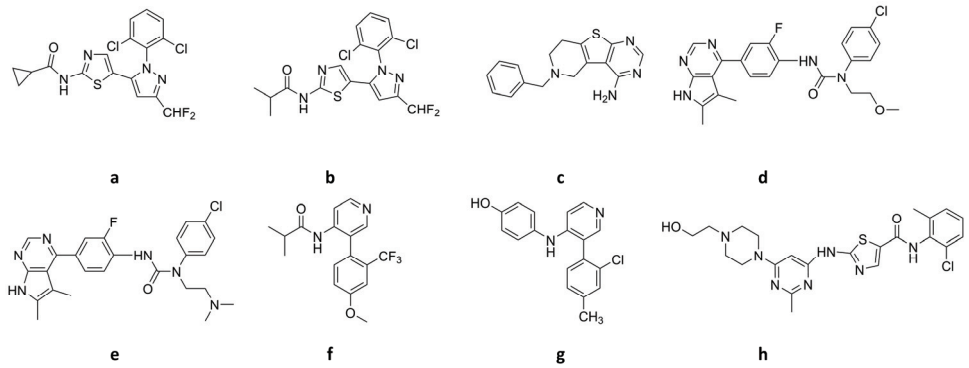

Fig. 1. Structures of some Limk1 inhibitors.

In this study, to design more Limk1 inhibitors, a 3D-QSAR model was firstly constructed based on aminothiazole Limk1 inhibitors reported by Charles *et al.*[16] Then, the binding requirements between ligand and receptor protein were

further explored through molecular docking study. Finally, based on the results, three theoretically superior compounds were designed and their ADME properties were predicted.

MATERIALS AND EXPERIMENTS

Software

In this paper, ChemDraw 19.0 was used to draw compounds, SYBYL X-2.0 was used to conduct 3D-QSAR models and Discovery Studio 2019 (DS) was used to do molecular docking.

Compounds source

The data used for quantitative structure-activity relationship study were reported by Charles *et al.*,[16] including 20 aminothiazole compounds. The given IC_{50} values were converted to pIC_{50} (pIC_{50} = –log IC_{50}) as the dependent variable. The structure and antagonistic activity of the compounds were listed in Table I. 16 inhibitors were selected as the training set for model building and 4 inhibitors (marked as *) were used as the test set for model evaluation in a random screening manner.

TABLE I. The studied Limk1 inhibitors and the corresponding experimental and predicted activity; * – inhibitors used as the test set for model evaluation in a random screening manner

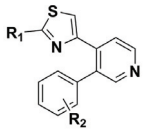

No.	R_1	R_2	pIC_{50}		
			Observed	Predicted	
				CoMFA	CoMSIA
1*	–NHPr	*o*-Cl	7.824	7.731	7.702
2		*m*-Cl	6.301	6.295	6.206
3		*p*-Cl	6.208	6.678	6.536
4		H	6.071	6.121	6.105
5		*o*-Me	7.086	6.979	6.840
6		*o*-*i*-Pr	5.481	5.429	5.597
7		*o*-CF_3	7.432	7.588	7.483
8		*o*-CF_3, *p*-OMe	7.886	7.603	7.719
9*	–NMePr	*o*-Cl	5.509	5.875	5.714
10	–NHEt	*o*-Cl	6.921	6.554	6.833
11	–NH-*i*-Bu	*o*-Cl	8.301	7.767	8.054
12	–NHCHMe(*S*)Ph	*o*-Cl	7.398	7.833	7.476
13	–NHCHMe(*R*)Ph	*o*-Cl	8.398	8.339	8.365
14	–NHPh	*o*-Cl	8.523	8.828	8.654
15	–NH-4-PhOH	*o*-Cl, *p*-Me	9.523	9.273	9.663
16	–NH_2	*o*-Cl	6.569	6.749	6.566
17*	–NHCOMe	*o*-Cl	7.699	7.517	7.137
18	–NHCO-*i*-Pr	*o*-Cl	8.523	8.919	8.732
19		*o*-Cl, *p*-Me	9.000	8.666	8.794
20*		*o*-CF_3, *p*-OMe	8.097	7.680	7.819

Molecular conformations generation

The drawn structures were put into the SYBYL X-2.0 form, the Tripos force field was chosen for energy optimization and Gasteiger-Hückel charges were imparted to the molecules. To get the lowest energy conformation, multi-search was used for conformation search. The search yielded 200 conformations for each molecule, which were saved in different databases, and the conformation with lowest energy from each database was selected for follow-up research.[16]

Molecular alignment

In order to clarify the structure-activity relationship, the most active compound **15** was selected as the template molecule. The "align database" function was then applied to align the train/test compounds with the common substructure respectively, as shown in Fig. 2.

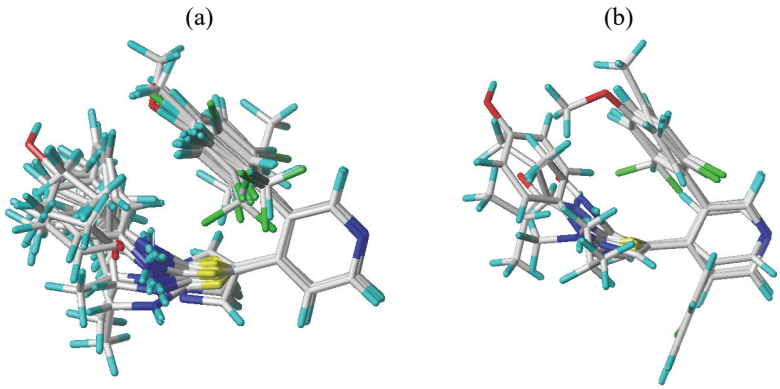

Fig. 2. a) The alignment of the training set. b) The alignment of the test set.

CoMFA and CoMSIA models construction

The CoMFA model describes two features: the steric and the electrostatic field; while the CoMSIA analysis has more exploratory capability: steric, electrostatic, hydrophobic, hydrogen bond donor and acceptor.

The lowest energy conformation of each compound in the previously saved database was selected. The pIC_{50} of each compound was used as the dependent variable, while the eigenvalues of CoMFA and CoMSIA were used as independent variables. Then the partial least-square (PLS) analysis was applied to establish the CoMFA and CoMSIA models. Firstly, the leave-one-out (LOO) cross-validation in PLS was used to obtain the maximum principal component value and cross-validation coefficient. After a reasonable maximum principal component value was obtained, a series of statistical parameters (Table I) were calculated through non-cross-validation under the condition of the maximum principal component value. Finally, the test set was used to validate the prediction ability of CoMFA and CoMSIA models from the external.

Molecular docking

The structure of the recently reported Limk1-staurosporine complex (PDB 3S95) was used and a series of very critical preparations of this protein, such as hydrogenation, charge addition and ligands deletion, were carried out in DS software using the Prepare Protein protocol.[17] The ATP pocket where the staurosporine is located was chosen as the docking pocket

with coordinates X = 45.2308, Y = 21.0287, Z = 68.0594, and a radius of 7.195037. Finally, the LibDock module was used in the docking process, while other parameters were kept as default.

ADME prediction

ADME prediction was performed using the online server http://www.swissadme.ch/,[18] a web-based ADME screening tool that predicts the drug-likeness of newly designed compounds to reduce waste of money and time in later drug development process.

RESULTS AND DISCUSSION

3D-QSAR model parameters

The reliability of the model was evaluated by the LOO cross-validated correlation coefficient, q^2, the non-validated correlation coefficient, r^2, the standard error of the estimated *SEE* and the F statistic. The predicted correlation coefficient, r^2_{pred}, was applied to validate the model's predictive power. The relevant values were listed in Table II.

TABLE II. Statistical parameters of 3D-QSAR models

Parameter						Contribution, %				
q^2	r^2	*ONC*	*F*	*SEE*	r^2_{pred}	*S*	*E*	*H*	*D*	*A*
CoMFA										
0.517	0.932	3	54.532	0.343	0.876	52.7	47.3	–	–	–
CoMSIA										
0.772	0.980	4	132.088	0.196	0.896	6.3	17.4	21.4	14.0	40.9

A model with $q^2 > 0.5$ is generally considered to be reliable and has good predictive power. The CoMFA model has 52.7 and 47.3 % of the steric and electrostatic fields, respectively, with optimal number of components (*ONC*) = 3, r^2 = = 0.932, q^2 = 0.517, *SEE* = 0.343 and r^2_{pred} = 0.876. The CoMSIA model has 6.3, 17.4, 21.4, 14 and 40.9 % of the steric, electrostatic, hydrophobic, hydrogen bond donor and hydrogen bond acceptor fields respectively. Its *ONC* = 4, r^2 = = 0.980, q^2 = 0.772, *SEE* = 0.196 and r^2_{pred} = 0.896. The training and test sets were regressed linearly on the values of the experimental pIC_{50} and the predicted pIC_{50} using a scatter plot. The resulting fitted curves were shown in Fig. 3, indicating that the CoMFA and CoMSIA models are stable and reliable.

Contour map analysis

CoMFA contour maps. The steric field contour map was shown in Fig. 4. As shown in Fig. 4a, the green and yellow contours distribute evenly in the R_1 region, which indicates that the substituted group with appropriate size in R_1 is beneficial to the activity (IC_{50} = 5 nM for **11** *vs.* 120 nM for **10** *vs.* IC_{50} = 270 nM for **16**). It is also observed that the benzene ring in the R_1 region is preferred to the alkyl substitution (IC_{50} = 3 nM for **14** *vs.* 120 nM for **10**). There are three big yellow contours in the R_2 region, which indicates that bulky groups are dis-

favored for Limk1 inhibition in this region. As shown in Fig. 4b, the activity of the compound decreases when there is a bulky group in the R_2 region (IC_{50} = 3300 nM for **6** *vs.* 850 nM for **4**). In general, groups with appropriate size in the R_1 region (where aromatic groups would be preferred over alkyl substitutions) can improve the activity, and when there are bulky groups in the R_2 region, the activity of the compound would decrease.

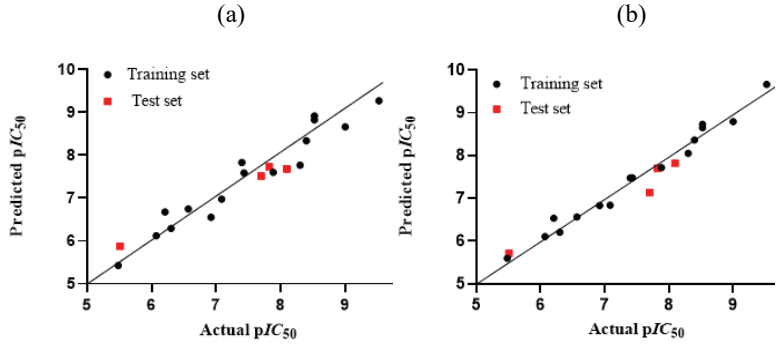

Fig. 3. Plots of actual versus predicted values. a) CoMFA model. b) CoMSIA model.

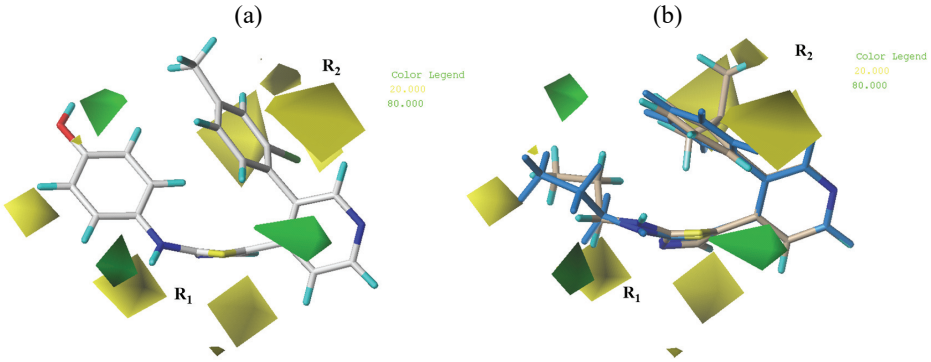

Fig. 4. Contour maps of CoMFA steric field (bulky groups are favored in the green regions and disfavored in the yellow regions). a) Compound **15** in steric field. b) Compound **4** (blue) and **6** (gray) in steric field.

The electrostatic field contour map was shown in Fig. 5.

As shown in Fig. 5a, there are both blue and red contours in the R_1 region, suggesting that groups with appropriate charge are favorable for Limk1 inhibition. For example, –NHCHMe(*R*)Ph (**13**), –NH-4-PhOH (**15**) and –NHCO-*i*-Pr (**19**) are all good for Limk1 inhibitory activity (IC_{50} = 4 nM for **13** *vs.* 0.3 nM for **15** *vs.* 1 nM for **19**). According to Fig. 5b, there is a blue contour in the R_2 region, which indicates that electropositive groups, such as $–CH_3$, are beneficial to inhibiting Limk1 (IC_{50} = 1 nM for **19** *vs.* 2 nM for **18**).

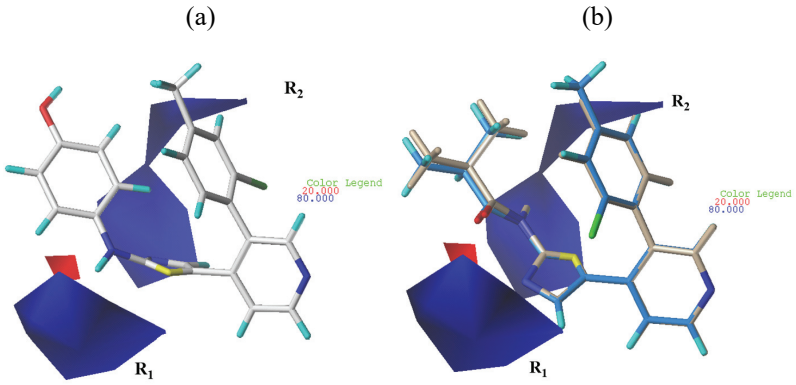

Fig. 5. Contour maps of CoMFA electrostatic field (electropositive groups are favored in the blue regions, and electronegative groups are favored in the red regions). a) Compound **15** in electrostatic field. b) Compound **19** (blue) and **18** (gray) in electrostatic field.

CoMSIA contour maps. As shown in Fig. 6, compound **15** was put into contour maps of CoMSIA model. Since the steric field accounts for only 6.3 %, the effect is negligible. In Fig. 6a, the R_2 region is surrounded by the blue contours, same as the CoMFA electrostatic field. But unlike CoMFA, the R_1 region has a small red contour, indicating that the introduction of $–NO_2$, –F, –Cl, *etc*. may contribute to the activity increase.

In Fig. 6b, no contours appear in the R_1 region, indicating that the substituent groups in this region are not sensitive to hydrophilic and hydrophobic interactions. The R_2 region is surrounded by a white contour, which means that the introduction of hydrophilic groups can enhance the inhibitory activity, such as –OH and $–NH_2$. In Fig. 6c, the N atom in the R_1 region attached to the aminothiazole ring is surrounded by a cyan contour, suggesting that the alkylated N atom is less active than the unsubstituted –NH (IC_{50} = 3100 nM for **9** *vs.* 270 nM for **16**). As shown in Fig. 6d, the addition of groups with a hydrogen bond donor or acceptor in the R_2 region has no effect on the activity. However, the magenta and red contours uniformly wrap the N atom in the R_1 region, indicating that groups with a hydrogen bond donor and acceptor, such as –OH and $–NH_2$, can both enhance the activity.

Molecular docking

3D-QSAR models can not directly show the interactions between ligands and the receptors. To further investigate the effect of the substituted groups in the R_1 and R_2 regions on the activity, the molecular docking was conducted.

In order to test the reliability of the molecular docking method, the original ligand was extracted and re-docked. The conformation with the highest score was selected to overlap with the original conformation. The original and the experi-

mental conformations are superimposed well, and the *RMSD* value is 0.07614 nm (< 0.2 nm), indicating that the docking method used is reliable.[19]

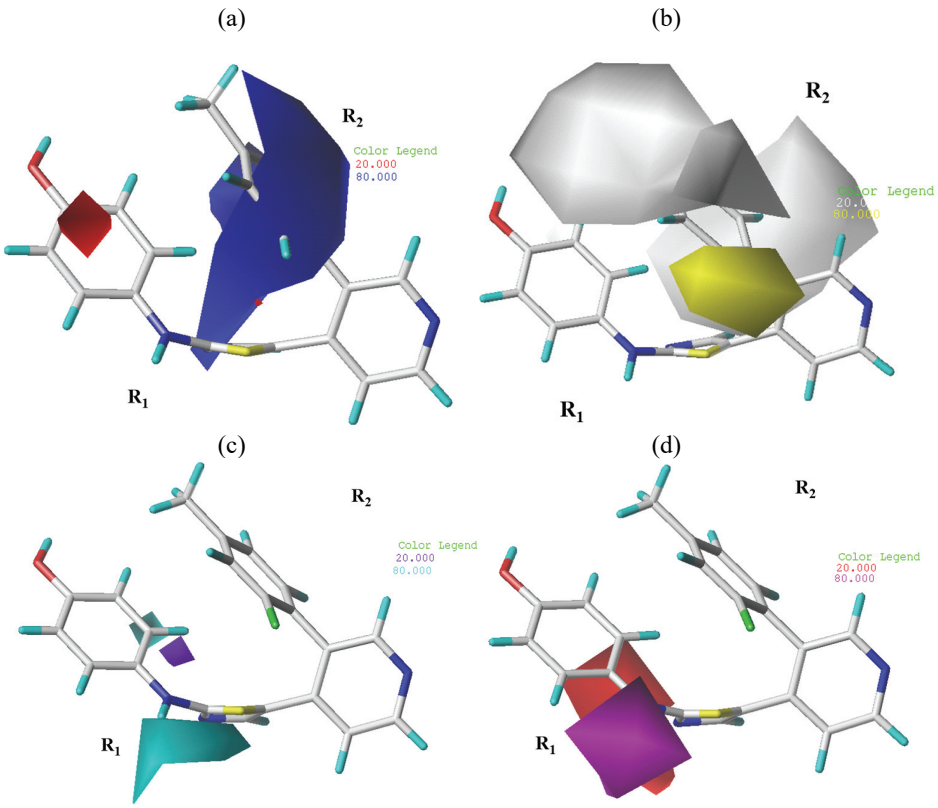

Fig. 6. Contour maps of the CoMSIA model (hydrophobic groups are favored in the yellow regions and disfavored in the white regions. H-bond donor groups are favored the cyan regions and disfavored in the purple regions. H-bond acceptor groups are favored in the magenta regions and disfavored in red regions). a) Electrostatic field. b) Hydrophobic field. c) Hydrogen bond donor field. d) Hydrogen bond acceptor field.

Twenty aminothiazole Limk1 inhibitors were docked to the protein ATP binding site. The top six scoring compounds were listed in Table III. It can be noticed that the compounds generally scored higher when there was a benzene ring in the R_1 region, which may be due to the hydrophobic interaction between the benzene ring and the surrounding amino acid residues. The active pocket in the R_1 region remains unfilled, suggesting that substituents with appropriate size could improve the interactions. These are consistent with the results of the 3D--QSAR model analysis. In addition, more than half of the inhibitors interacted with amino acids Leu345, Ala353, Val366, Lys368, Leu397, Tyr415, Ile416, Leu467 and Ala477, suggesting that these nine amino acids may be the primary

amino acids for protein-ligand interaction. 3D and 2D plots of the docking results for the highest scoring compound **12** and the most active compound **15** were shown in Fig. 7. Amino acid Ile416 formed hydrogen bond at distances of 0.183 nm (–N···H–) and 0.248 nm (–H···O–) with compounds **12** and **15**, respectively, and this hydrogen bond was considered to be essential for the inhibitory activity.[17] It can also be observed that compound **12** formed a hydrogen bond with Ile416 by the "N" in the pyridine ring on its common skeleton, while **15** formed a hydrogen bond with Ile416 by a substituted hydroxyl group in the R_1 region. When modifying the substituents in the R_1 and R_2 regions, the effect on the conformation of the compound should be considered.

TABLE III. Results of docking fraction study on the interaction of compounds and Limk1 protein

No.	Docking score	Mode of action			
		Hydrogen bonds	Hydrophobic	Pi-Anion	Pi-Alkyl
12	99.7584	Ile416	Glu384, Phe411, Asp478, Leu397, Thr413	–	Lys368, Ala477, Ala353
13	98.9368	–	Glu414, Gly419, Tyr415, Thr413, Phe411, Asn465	–	Leu345, Leu467, Ala477, Ala353, Leu397, LYS368
8	93.7566	Asp478	Ile416, Glu414	–	Ala353, Ala477, Leu397, Leu345, Leu467
7	92.0749	Asp478, Lys368	Glu414	–	Leu467, Leu345, Val366
20	91.7253	Asp478	Val366, Met367, Gly419	Asp478	Leu467, Ile416, LEU345
15	90.8909	Ile416	Lys368, Thr413, Phe411	Asp478	Val366, Leu467, Ala353, Leu397, Ala477

New compounds design

As shown in Fig. 8, three theoretically active Limk1 inhibitors were designed using compound **12** as the template based on the results analyses of contour maps and molecular docking. The results of activity prediction and molecular docking were shown in Table IV. The conformation of the new compound was overlapped with that of compound **12**, respectively, and the *RMSD* values showed that the conformation of the newly designed compound had little change compared with that of compound **12**. All of them scored better than **12**, forming hydrogen bonds with Ile416 (bond length = 0.203 nm for **N1**, 0.213 nm for **N2** and 0.201 nm for **N3**). Compound **N3** scored highest, probably due to the additional hydrogen bonding with Glu384. Overall, the newly designed compounds have high predicted activity and scores, indicating successful compound design.

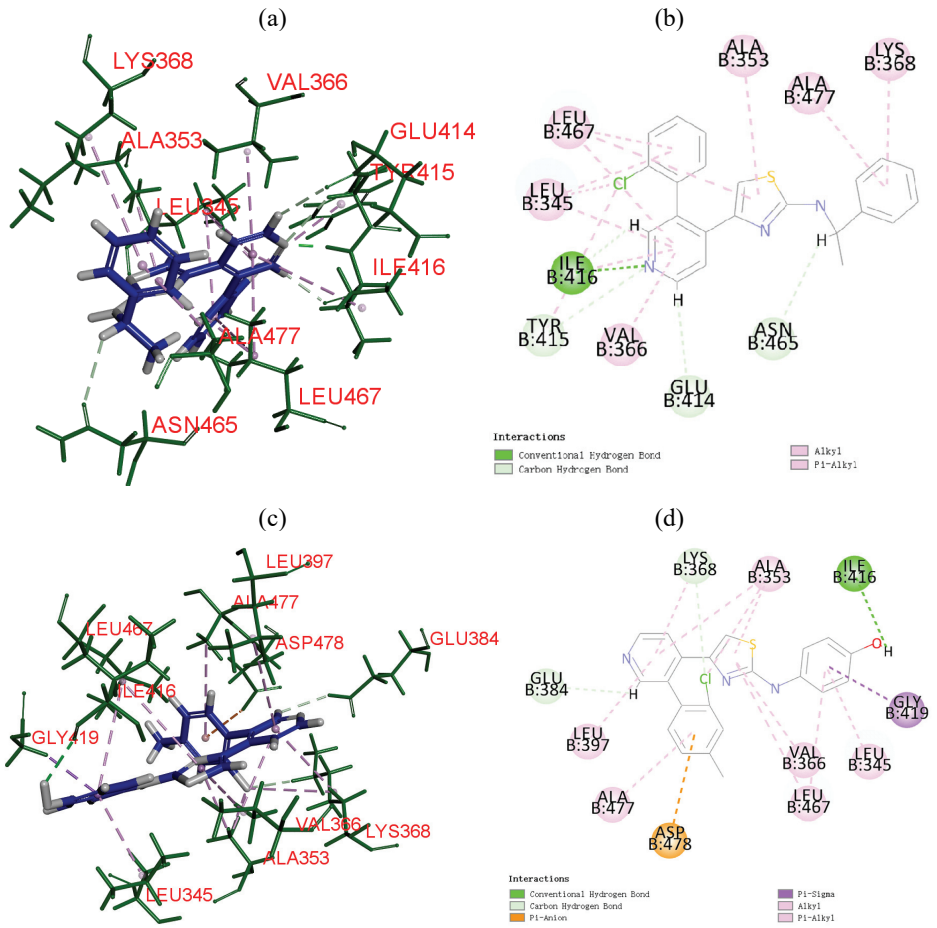

Fig. 7. a) 3D interaction map of compound **12**; b) 2D interaction map of compound **12**; c) 3D interaction map of compound **15**; d) 2D interaction map of compound **15**.

TABLE IV. The results of activity prediction and molecular docking

Compd.	Pred. IC_{50} / nM		Docking score	Critical amino acid residues	*RMSD* / nm
	CoMFA	CoMSIA			
N1	16.2	18.5	104.469	Ile416	0.1459
N2	23.4	32.6	104.290	Ile416	0.3144
N3	25.6	34.2	109.319	Ile416, Glu384	0.2092

ADME forecast results and analysis

The ADME projections were listed in Table V. The newly designed compounds have better lipid-water partition coefficient and solubility compared to compound **12**. They all have superior Human intestinal absorption, which indicates that the compounds have good absorption property. **N1** and **N2** are both meta-

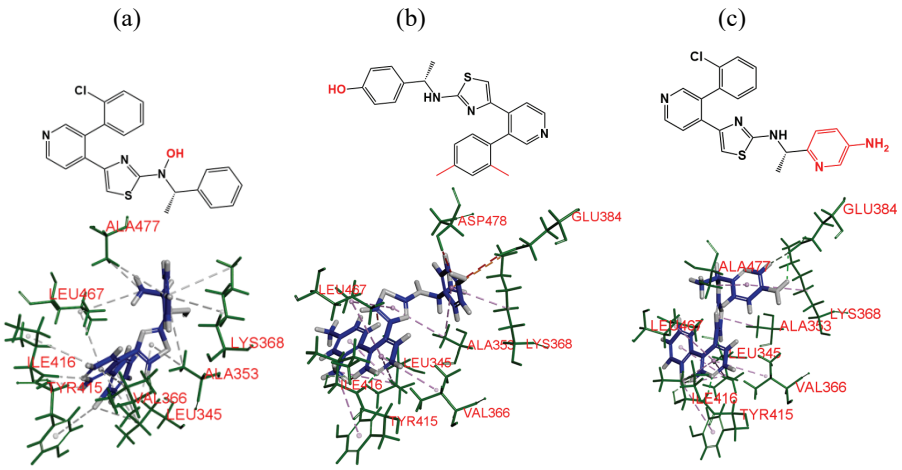

Fig. 8. a) 3D interaction map and structure of **N1**; b) 3D interaction map and structure of **N2**; c) 3D interaction map and structure of **N3**.

TABLE V. The results of predicted ADME; log *S* scale: insoluble < –10 < poorly < –6 < moderately < –4 < soluble < –2 very < 0 < highly; HIA: human intestinal absorption; BBB: blood brain barrier penetration; CYP450 inhibitor subtypes: CYP4501A2, CYP4502C19, CYP4502C9, CYP4502D6, CYP4503A4

No	MW	log $P_{o/w}$ (<5)	log *S*	Pharmacokinetics			Drug likeness
				HIA	BBB	CYP450 inhibitor	
12	391.92	5.25	-6.36	High	No	Yes	Yes
N1	407.92	4.96	-6.21	High	No	Yes	Yes
N2	401.52	4,94	-6.22	High	No	Yes	Yes
N3	407.92	3.94	-5.36	High	No	No	Yes

bolized by inhibitors of CYP450 subtypes 1A2, 2C19, 2C9, 2D6 and 3A4, while **N3** is not metabolized by 1A2. The drug-like properties were evaluated using Lipinski's rule and the results were all "Yes" which indicates that they all have good drug-like properties. From these results, it is clear that the newly designed compounds have good bioavailability and drug-like properties and are expected to be novel Limk1 inhibitors.

CONCLUSIONS

Limk1 is a target of great concern, but until now there has been no marketed drug for this target. In this paper, the reliable CoMFA and CoMSIA models were established based on a series of aminothiazole Limk1 inhibitors. The contour maps of the CoMFA and CoMSIA models demonstrate the key groups that influence the activity of Limk1 inhibitors. Molecular docking further indicates that Ala477, Glu384, Leu397, Lys368, Ala353, Leu467, Val366, Ile416 and Leu345 are the main amino acids for aminothiazole inhibitors to interact with Limk1 pro-

tein and hydrophobic interactions may increase the affinity. Based on these analyses, three novel aminothiazoles with potential Limk1 inhibitory activity with good feasibility and ADME evaluation results were designed.

Acknowledgements. The authors are grateful for Jiangsu Education Department (JSSCBS20211302), Jiangsu Institute of Marine Resources Development (JSIMR202015) and Jiangsu Ocean University for financial and technical support.

ИЗВОД

3D-QSAR И СТУДИЈЕ МОЛЕКУСКИМ ДОКИНГОМ ИНХИБИТОРА АМИНОТИАЗОЛ Lim КИНАЗЕ 1

JING-XUAN HOU, QING-SHAN GU, MEI-QI SHI, HUI GAO, LU ZHENG и QING-KUN WU

School of Pharmacy, Jiangsu Ocean University, Jiangsu, 320000, P.R. China

Lim киназа (Limk), као значајан цитоскелетни регулатор, има значајну улогу у испољавању канцера и нервним болестима. Limk1 је члан Limk породице, која је углавном укључена у инвазији и метастази туморских ћелија и ненормално је испољена у ћелијама различних ткива канцера. У овом раду је употребљена серија Limk1 инхибитора са аминотиазолским скелетом да би се рачунарским приступом дизајнирали моћни и ефикасни Limk1 инхибитори. Прво је конструисан 3D-QSAR модел, и CoMFA и CoMSIA су имали велику способност корелисања и претсказивања. Онда су путем молекулског докинга анализиране интеракције између лиганда и рецептора. На крају, сагласно 3D-QSAR анализи и резултатима молекулског докинга, дизајнирана су три једињења са теоретски бољом активношћу.

(Примљено 10. маја, ревидирано 14. јула, прихваћено 23. септембра 2022)

REFERENCES

1. K. Yoshioka, V. Foletta, O. Bernard, K. Itoh, *Proc. Natl. Acad. Sci.* **100** (2003) 7247 (https://doi.org/10.1073/pnas.1232344100)
2. C. Prunier, R. Prudent, R. Kapur, K. Sadoul, L. Lafanechère, *Oncotarget* **8** (2017) 41749 (https://doi.org/10.18632/oncotarget.16978)
3. F. Yi, J. Guo, D. Dabbagh, M. Spear, S. He, K. Kehn-Hall, J. Fontenot, Y. Yin, M. Bibian, C. M. Park, *J. Virol.* **91** (2017) e02418-16 (https://doi.org/10.1128/JVI.02418-16)
4. F. Manetti, *Drug Discov. Today* **17** (2012) 81 (https://doi.org/10.1016/j.drudis.2011.08.004)
5. A. Jayo, M. Parsons, J. C. Adams, *BMC Biol.* **10** (2012) 1 (https://doi.org/10.1186/1741-7007-10-72)
6. D. H. Vlecken, C. P. Bagowski, *Zebrafish* **6** (2009) 433 (https://doi.org/10.1089/zeb.2009.0602)
7. O. Bernard, *Int. J. Biochem. Cell Biol.* **39** (2007) 1071 (https://doi.org/10.1016/j.biocel.2006.11.011)
8. P. Chen, M. Zeng, Y. Zhao, X. Fang, *Oncol. Rep.* **32** (2014) 2070 (https://doi.org/10.3892/or.2014.3461)
9. J. Zhou, R. Liu, C. Luo, X. Zhou, K. Xia, X. Chen, M. Zhou, Q. Zou, P. Cao, K. Cao, *Cancer Biol. Ther.* **15** (2014) 1340 (https://doi.org/10.4161/cbt.29821)

10. P. Ross-Macdonald, H. de Silva, Q. Guo, H. Xiao, C.-Y. Hung, B. Penhallow, J. Markwalder, L. He, R. M. Attar, T. Lin, *Mol. Cancer Ther.* **7** (2008) 3490 (https://doi.org/10.1158/1535-7163.MCT-08-0826)
11. B. E. Sleebs, G. Nikolakopoulos, I. P. Street, H. Falk, J. B. Baell, *Bioorg. Med. Chem. Lett.* **21** (2011) 5992 (https://doi.org/10.1016/j.bmcl.2011.07.050)
12. Y. Yin, K. Zheng, N. Eid, S. Howard, J.-H. Jeong, F. Yi, J. Guo, C. M. Park, M. Bibian, W. Wu, *J. Med. Chem.* **58** (2015) 1846 (https://doi.org/10.1021/jm501680m)
13. M. D. Charles, J. L. Brookfield, T. C. Ekwuru, M. Stockley, J. Dunn, M. Riddick, T. Hammonds, E. Trivier, G. Greenland, A. C. Wong, *J. Med. Chem.* **58** (2015) 8309 (https://doi.org/10.1021/acs.jmedchem.5b01242)
14. K. Mardilovich, M. Baugh, D. Crighton, D. Kowalczyk, M. Gabrielsen, J. Munro, D. R. Croft, F. Lourenco, D. James, G. Kalna, *Oncotarget* **6** (2015) 38469 (https://doi.org/10.18632/oncotarget.6288)
15. M. Zhang, J. Tian, R. Wang, M. Song, R. Zhao, H. Chen, K. Liu, J.-H. Shim, F. Zhu, Z. Dong, *Front. Cell Dev. Biol.* (2020) 1361 (https://doi.org/10.3389/fcell.2020.556532)
16. X. Xu, B. Xu, X. Wang, & J. Li, *J. Mol. Struct.* **1201** (2020) 127128 (https://doi.org/10.1016/j.molstruc.2019.127128)
17. M. Sari-Hassoun, M.-J. Clement, I. Hamdi, G. Bollot, C. Bauvais, V. Joshi, F. Toma, A. Burgo, M. Cailleret, M. C. Rosales-Hernández, *Biochem. Pharmacol.* **102** (2016) 45 (https://doi.org/10.1016/j.bcp.2015.12.013)
18. A. Daina, O. Michielin, V. Zoete, *Sci. Rep.* **7** (2017) 1 (https://doi.org/10.1038/srep42717)
19. W. J. Egan, K. M. Merz, J. J. Baldwin, *J. Med. Chem.* **43** (2000) 3867 (https://doi.org/10.1021/jm000292e).